APPsα rescues impaired Ca^{2+} homeostasis in APP- and APLP2-deficient hippocampal neurons

Susann Ludewig[a,b], Ulrike Herrmann[a], Kristin Michaelsen-Preusse[a], Kristin Metzdorf[a,b], Jennifer Just[a], Charlotte Bold[c], Ulrike C. Müller[c], and Martin Korte[a,b,1]

[a]Department of Cellular Neurobiology Zoological Institute, Technische Universität Braunschweig, 38106 Braunschweig, Germany; [b]Neuroinflammation and Neurodegeneration, Helmholtz Centre for Infection Research, 38124 Braunschweig, Germany; and [c]Department of Functional Genomics, Institute for Pharmacy and Molecular Biotechnology, Heidelberg University, 69120 Heidelberg, Germany

Edited by Mu-ming Poo, Chinese Academy of Sciences, Shanghai, China, and approved May 19, 2021 (received for review June 4, 2020)

Alterations in Ca^{2+} homeostasis have been reported in several in vitro and in vivo studies using mice expressing the Alzheimer's disease–associated transgenes, presenilin and the amyloid precursor protein (APP). While intense research focused on amyloid-β–mediated functions on neuronal Ca^{2+} handling, the physiological role of APP and its close homolog APLP2 is still not fully clarified. We now elucidate a mechanism to show how APP and its homolog APLP2 control neuronal Ca^{2+} handling and identify especially the ectodomain APPsα as an essential regulator of Ca^{2+} homeostasis. Importantly, we demonstrate that the loss of APP and APLP2, but not APLP2 alone, impairs Ca^{2+} handling, the refill of the endoplasmic reticulum Ca^{2+} stores, and synaptic plasticity due to altered function and expression of the SERCA-ATPase and expression of store-operated Ca^{2+} channel–associated proteins Stim1 and Stim2. Long-term AAV-mediated expression of APPsα, but not acute application of the recombinant protein, restored physiological Ca^{2+} homeostasis and synaptic plasticity in APP/APLP2 cDKO cultures. Overall, our analysis reveals an essential role of the APP family and especially of the ectodomain APPsα in Ca^{2+} homeostasis, thereby highlighting its therapeutic potential.

Alzheimer's disease | APP | Ca2+ homeostasis | synaptic plasticity

Neuronal calcium (Ca^{2+}) signaling is an important prerequisite for normal cell function, as impairments in Ca^{2+} handling have been implicated in a variety of neurodegenerative disorders including Alzheimer's disease (AD) (1–4). Under resting conditions, cytosolic [Ca^{2+}] is maintained at low nanomolar concentrations. Ca^{2+} entry into the cytosol is strictly regulated and originates from the extracellular fluid either via the plasma membrane through ligand-gated, voltage-gated (VGCC), and store-operated (SOCC) channels as well as Ca^{2+} exchangers or from intracellular stores such as the endoplasmic reticulum (ER) and mitochondria (5, 6). Fluctuations in [Ca^{2+}] influence enzymatic signaling cascades, leading even to alterations in gene transcription, and are therefore crucial for the plasticity of neuronal networks. Synaptic plasticity as a cellular correlate of learning and memory formation is indeed impaired in AD and amyloid precursor protein (APP)-deficient mice (for a review, see refs. 7 and 8) and has been linked to dysregulated Ca^{2+} homeostasis (9–11). In this regard, it is interesting to note that while aged APP-knockout (KO) mice exhibit impaired long-term potentiation (LTP) and impaired hippocampus-dependent learning (12–14), these alterations are absent in young APP-KO mice as well as in mice with a deletion of the close APP homolog APLP2 (15, 16). Additionally, already in young mice, the forebrain-specific KO of APP on a constitutive global APLP2 $^{-/-}$ background (NexCre cDKO) results in a pronounced deficit in the induction and maintenance of LTP as well as in compromised hippocampus-dependent memory tasks. These findings in NexCre cDKO mice, contrasting the age-dependent impairments in APP-KO mice, possibly indicate a functional compensation in the respective single KOs of APLP2 or young APP mice. Furthermore, NexCre cDKO mice show disturbances during paired-pulse facilitation (PPF) and the phase of post-tetanic potentiation of LTP, processes associated with short-term plasticity (STP) (17). STP is a form of plasticity driven by changes in the activation of Ca^{2+} sensor kinases and in a series of Ca^{2+}-dependent processes such as release probability, recycling, and content of synaptic vesicles at the presynapse (18). At the postsynapse, LTP depends on a robust and relatively short Ca^{2+} influx through *N*-methyl-D-aspartate receptors (NMDARs). In general, APP family members are well known to regulate activity-dependent synaptic plasticity (7, 19), possibly affecting intracellular [Ca^{2+}] by regulating the postsynaptic cell-surface expression of NMDARs as well as its subunit composition (20–23). Previous studies addressing the role of full-length APP in Ca^{2+} homeostasis, mainly performed in nonneuronal cell types, revealed a dysregulation of Ca^{2+} signaling in APP-KO astrocytes (24–26) and fibroblasts (27) as well as increased ER [Ca^{2+}] in carcinoma (11) and neuroblastoma cells with altered SOCC activity (28), while neuronal-related Ca^{2+} activity has mainly been investigated with respect to AD. Mutations in presenilins (PS) and APP causing familial AD affect ER Ca^{2+} signaling by overloading ER stores (29, 30), especially in neurons that are in close proximity to amyloid-β (Aβ) plaques (31), and reduce the expression of stromal interaction molecule 2 (STIM2) that further compromise SOCC (32). The intracellular increase in [Ca^{2+}] is attributed to pores in the cell membrane formed by Aβ (33, 34) or overactivation of mGluR5 receptors (30). Aβ peptides are APP cleavage products resulting from sequential processing by β- and y-secretase (35, 36). In the competing nonamyloidogenic APP processing pathway, α-secretase cleavage within the Aβ region liberates

Significance

Ca^{2+} dysfunction is correlated to the progression of Alzheimer's disease; mechanistic insight into the physiological role of the amyloid precursor protein (APP) for Ca^{2+} homeostasis is still missing. We demonstrate that loss of APP and its homolog APLP2, but not APLP2 alone, impairs Ca^{2+} handling and synaptic plasticity because of altered function of endoplasmic reticulum Ca^{2+} stores caused by altered expression and function of the SERCA-ATPase as well as by expression of store-operated Ca^{2+} channel–associated proteins Stim1 and Stim2. Long-term expression of the APPsα ectodomain restored physiological Ca^{2+} homeostasis, protein expression, and synaptic plasticity in APP/APLP2 cDKO cultures, emphasizing the role of the APP family and especially of the ectodomain APPsα in Ca^{2+} homeostasis, thereby highlighting its therapeutic potential.

Author contributions: U.C.M. and M.K. designed research; S.L., U.H., K.M., and J.J. performed research; C.B. contributed new reagents/analytic tools; S.L., U.H., K.M.-P., K.M., and C.B. analyzed data; and S.L., K.M.-P., U.C.M., and M.K. wrote the paper.

The authors declare no competing interest.

This article is a PNAS Direct Submission.

[1]To whom correspondence may be addressed. Email: m.korte@tu-bs.de.

This article contains supporting information online at https://www.pnas.org/lookup/suppl/doi:10.1073/pnas.2011506118/-/DCSupplemental.

Published June 25, 2021.

the neurotrophic ectodomain APPsα (37), which is assumed to mitigate Aβ-induced toxic effects (7, 38). Recently, we identified APPsα as a crucial domain mediating the function of the APP full-length protein with regard to synaptic plasticity as well as learning and memory formation (17, 39). Furthermore, we showed that virus-mediated expression of murine APPsα restored LTP as well as PPF in aged AD model (APP/PS1ΔE9) mice (38), which has recently been confirmed using the human APPsα (40). Here, we addressed the important question of if the APP family and especially APPsα might also regulate neuronal Ca^{2+} homeostasis under physiological conditions in neurons. In this respect, we establish APP and APLP2 as important players regulating somatic Ca^{2+} transients. Our results indicate that impaired Ca^{2+} handling may arise from increased SERCA-ATPase expression and altered activity at ER Ca^{2+} stores as well as increased levels of the SOCC-associated proteins Stim1 and Stim2. Moreover, we identify APPsα as an essential functional domain for Ca^{2+} homeostasis as its re-expression rescued impaired Ca^{2+} homeostasis and protein expression in neurons of APP/APLP2 cDKOs.

Results

A previous investigation of conditional APP/APLP2-deficient mice (NexCre cDKO) and their littermate controls (APLP2-KO) revealed impaired LTP, L-LTP, and STP for the conditional mutants (17, 39). Impaired intracellular Ca^{2+} handling that derives either from an increased and sustained entry of Ca^{2+} through membrane channels or from an inefficient clearance of Ca^{2+} from the cytosol can lead to an imbalance in processes of synaptic plasticity, like the induction of LTP versus LTD, and thereby interfere with memory formation (1). Thus, we first asked if disturbed Ca^{2+} handling might underlie the observed phenotypes.

Disturbed Ca^{2+} Handling and Impaired cLTP in NexCre cDKOs due to Up-Regulated ER Ca^{2+} Store Activity. We explored Ca^{2+} signaling using the Fura2-AM indicator in NexCre cDKO ($APP^{flox/flox}$APLP2) and littermate (LM) control (APLP2-KO) hippocampal cultures, applying a chemical induction protocol to evoke NMDAR-dependent LTP (cLTP), comparable to electrical stimulation (*SI Appendix*, Fig. S1). Upon cLTP induction (1 mM Glycine, 1 μM Strychnine), cultured neurons showed an increase in the amplitude of spontaneous global Ca^{2+} transients compared to baseline activity [Fig. 1 *A* and *D*, two-way repeated measures (RM) ANOVA time, $F(4, 88) = 34{,}16$, $P < 0.001$]. However, already during the baseline recording it became apparent that amplitudes of spontaneous Ca^{2+} transients were significantly smaller in NexCre cDKO mice at t−20 [Fig. 1*A*, two-way RM ANOVA time × genotype, $F(4, 88) = 3{,}596$, $P = 0.0092$; post hoc Fisher's least significant difference [LSD], $p(t{-}20) = 0.011$] compared to LMs. To confirm that the defect in the lower Ca^{2+} concentration in the NexCre cDKOs is not masked by the use of Fura2-AM as a high-affinity Ca^{2+} dye, we additionally used Fura-FF as a low-affinity Ca^{2+} indicator. The measurements of spontaneous Ca^{2+} activity of Fura-FF–labeled neurons revealed a significant decrease in the amplitude of Ca^{2+} transients in NexCre cDKO cultures transduced with AAV-Venus compared to LM controls [*SI Appendix*, Fig. S2*A*; two-way ANOVA genotype, $F(1,124) = 7.862$, $P = 0.006$; post hoc Fisher's LSD, p(Venus) = 0.016]. In line with the previously described tetra burst stimulus (TBS)-LTP deficit in hippocampal slices (17), the amplitude of cLTP-induced Ca^{2+} transients was overall significantly reduced between genotypes at imaging time points t10 to t40 and by trend at t0 [Fig. 1*A*, post hoc Fisher's LSD, $p(t0) = 0.0664$, $p(t10) < 0.001$, $p(t40) = 0.0014$]. Under conditions in which Ca^{2+} transients were normalized to amplitudes of spontaneous Ca^{2+} transients at the baseline level, both the LM control and NexCre DKOs showed an increase in intracellular [Ca^{2+}] by a comparable amount upon cLTP induction. There was even a slight temporary increase in the amplitude of Ca^{2+} transients in NexCre cDKO at t0, although not significantly different from the LM control [Fig. 1*A*', two-way RM ANOVA time × genotype, $F(3, 69) = 3.018$, $P = 0.036$; post hoc Fisher's LSD, $p(t0) = 0.163$]. Thus, the difference in Fura2-AM ratios resulted from smaller intracellular Ca^{2+} levels already before stimulation, indicating impaired Ca^{2+} handling under baseline conditions. As depicted in the example raw traces (Fig. 1*D*), LMs as well as NexCre cDKO neurons showed a reduction in Ca^{2+} transient frequency following cLTP induction that we attribute to network synchronization. Overall, we found in none of our analyses using the cLTP protocol different neuronal firing induced Ca^{2+} transients at any imaging time points between analyzed genotypes.

Next, we confirmed that the glycine-induced cLTP in NexCre cDKO and LM controls is NMDAR dependent using (2R)-amino-5-phosphonopentanoate (APV) (Fig. 1 *B* and *B*'). Inhibiting NMDARs with APV prevented the induction of cLTP in both genotypes as expected (Fig. 1*B*'). The comparison of Fura2-AM ratios between genotypes showed again a significant reduction for each time point in NexCre cDKOs [Fig. 1*B*, two-way RM ANOVA genotype, $F(1, 23) = 12.320$, $P = 0.002$; post hoc Fisher's LSD, $p(t{-}20) = 0.010$, $p(-10) = 0.020$, $p(0) = 0.067$, $p(10) = 0.002$, $p(40) = 0.013$]. At phases of spontaneous activity, elevations in cytosolic [Ca^{2+}] are rigorously regulated and originate either from intracellular stores or the extracellular space by receptor-, voltage-, and store-operated channels as well as Ca^{2+} exchangers (5), which could be responsible for significantly lower baseline Ca^{2+} transients in NexCre cDKO cultures.

To decipher the mechanism of Ca^{2+} handling change, we examined the potential role of VGCCs for elevations in intracellular [Ca^{2+}]. In this respect, alterations have been reported in the activity of L-type VGCCs (41) during aging and AD (42, 43) (see Fig. 7). To follow this lead, we applied a selective L-type VGCC inhibitor nifedipine (10 μM) together with glycine and strychnine during cLTP induction (*SI Appendix*, Fig. S2 *B* and *C*). Nifedipine treatment prevented a significant increase in the amplitude of Ca^{2+} transients in LM cultures as well as in NexCre cDKOs upon stimulation with no differences between genotypes. As a next step, we examined the second main source of cytoplasmic Ca^{2+} entry, the ER Ca^{2+} stores. Therefore, we blocked the reuptake of Ca^{2+} via the SERCA-ATPase into the ER by coapplication of cyclopiazoic acid (CPA, 10 μM) together with glycine and strychnine (Fig. 1 *C* and *C*' and also see Fig. 7). The analysis revealed that in LM neurons, the significant increase in Ca^{2+} amplitudes upon cLTP induction seen in Fig. 1*A* was largely abolished over time. Strikingly, the blocking of SERCA activity in NexCre cDKO neurons resulted in a highly significant increase in Ca^{2+} amplitudes recorded at t0 compared to global spontaneous Ca^{2+} transients under baseline conditions [Fig. 1*C*, two-way RM ANOVA time × genotype, $F(4, 40) = 3.585$, $P = 0.014$; post hoc Fisher's LSD, $p(t{-}20) = 0.031$, $p(0) = 0.028$]. Furthermore, CPA-treated NexCre cDKO cells reached values comparable to those observed following cLTP induction in LM neurons at t0 [ratio t0(LM) = 0.646 ± 0.05 versus ratio t10(NexCre cDKO) = 0.644 ± 0.06], indicating that the ER itself might be affected in APP/APLP2 mutants. The significant increase in Ca^{2+} ratios for NexCre cDKO cultures upon cLTP became even more obvious when the values were normalized to baseline Fura2-AM ratios [Fig. 1*C*', two-way RM ANOVA time × genotype, $F(3, 30) = 3.788$, $P = 0.020$; post hoc Fisher's LSD, $p(t0) = 0.047$]. Notable, as CPA is a reversible blocker and washed out following t0, a significant decrease of Ca^{2+} ratios was seen for t10 and t40 [Fig. 1*C*', two-way RM ANOVA time, $F(1.432, 14.320) = 11.680$, $P = 0.002$; post hoc Fisher's LSD, $p(t10) = 0.034$, $p(t40) = 0.029$] when compared to t0 in NexCre cDKO neurons, preventing stable increase in cLTP.

Based on the results of altered SERCA-ATPase activity during cLTP induction, we next investigated ER Ca^{2+} dynamics upon 5 min CPA treatment using the ER-GCaMP6-150 Ca^{2+} indicator (44) (Fig. 1*E*). As shown in Fig. 1*E*, NexCre cDKO neurons

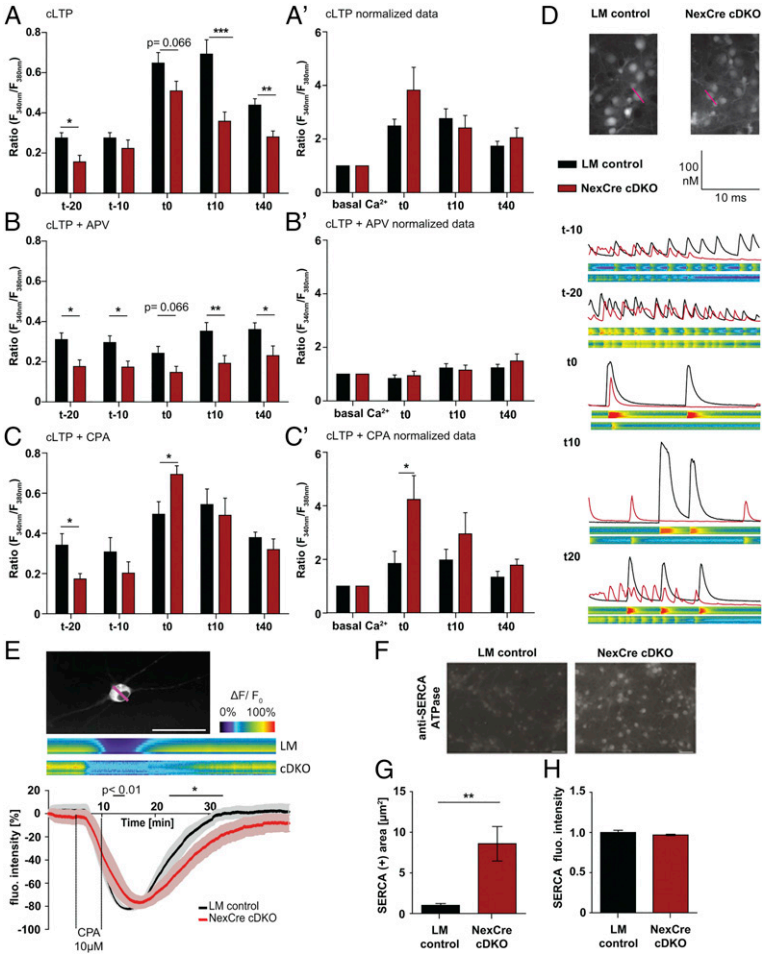

Fig. 1. Disturbed Ca^{2+} homeostasis and impaired cLTP in NexCre cDKO cultures. (*A*–*C*) Changes in Fura2-AM/Ca^{2+} fluorescence in primary embryonic hippocampal neurons of LM control (black bars) and NexCre cDKO (red bars) upon cLTP stimulation by glycine and strychnine (Gly/Stry). Imaging time points t−20 and t−10 reflect changes when cells were spontaneously active, whereas t0–t40 depict the quantification of relative Ca^{2+} changes upon Gly/Stry stimulation with or without additional drug application. (*A*) Following cLTP, the amplitude of Ca^{2+} transients were observed in both genotypes. NexCre cDKO cultures (n = 10/N = 7) compared to littermate controls (n = 14/N = 7). (*A′*) Normalization of Fura2-AM/Ca^{2+} fluorescence changes to pooled basal activity at t−20 and t−10. (*B*) Coapplication of Gly/Stry and APV (NMDAR inhibitor) prevented the significant Ca^{2+} increase in NexCre cDKO (n = 11/N = 7) compared to the LM control (n = 14/N = 7) (*B′*) while normalized values depict unaltered behavior toward treatment. (*C*) cLTP induction and additional application of CPA (SERCA inhibitor) prevented an overall significant increase of relative Ca^{2+} levels in LM controls (n = 6/N = 6) while a significant defect in the reuptake of Ca^{2+} in the ER was observable in NexCre cDKOs (n = 6/N = 6). (*C′*) Normalized data show increased relative Ca^{2+} levels upon cLTP, which decreased continuously from t10 and t40. (*D*) Representative image of Fura2-AM/Ca^{2+} fluorescence of LM controls (*Left*) and NexCre cDKO (*Right*). Example traces for cLTP induction by Gly/Stry in LM controls (black trace) and NexCre cDKO (red trace) displayed in the field of view with pseudoline scan (pink line). Ca^{2+} traces depict somatic Ca^{2+} signal for timepoints before (t−20 and t−10) and after cLTP induction (t0 to t40) as a heat map in a color range of 0% Ca^{2+} in purple and 100% Ca^{2+} in red (LM controls: *Upper*; NexCre cDKO: *Lower*). (*E*) Representative image of an ER-GCaMP6-150 transfected neuron displayed with a pseudoline scan (*Upper*) depicting the somatic Ca^{2+} signal as a heat map in a color range of 0% Ca^{2+} in purple and 100% Ca^{2+} in red. NexCre cDKO neurons (red; n = 9/N = 4) show a delayed release of ER Ca^{2+} and refill of the ER Ca^{2+} pool upon 5 min CPA wash in compared to LM controls (black; n = 12/N = 4). (*F*–*H*) Anti-SERCA2 ATPase signal and (*F*) quantified area and (*G*) mean fluorescence intensity (*H*) of the protein (LM control: n = 15/N = 5; NexCre cDKO: n = 21/N = 7). (Scale bar, 50 µm.) Significances were plotted as *P < 0.05, **P < 0.01, and ***P < 0.001. Error bars indicate ± SEM, n = number of cultures, N = independent number of culture preparations. For illustration, all images were equally increased in brightness and contrast by the same absolute values.

exhibited a delayed release of the ER-Ca^{2+} pool and a significantly slower refill of the ER Ca^{2+} pool compared to LM cultures [Fig. 1*E*, two-way RM ANOVA time × genotype, $F(2{,}699, 51{,}300) = 35.40$, $P < 0.0001$; post hoc Fisher's LSD, p(12 to 14 min) < 0.05]. Moreover, the ER Ca^{2+} pool was emptied to a lower extent in mutants [minimum fluorescence intensity(LM) = 82.36 ± 1.331% versus minimum fluorescence intensity(NexCre cDKO) = 76.85 ± 5.173%]. Next, we quantified SERCA2 ATPase immunofluorescence using a threshold analysis (Fig. 1*F*). The area of SERCA-positive somata was approximately eightfold higher in NexCre cDKO compared to LM neurons (Fig. 1*G*, unpaired Student's t test, $P = 0.005$). Meanwhile, there was no difference between the two conditions in the mean values of fluorescence intensity of SERCA-ATPase (Fig. 1*H*).

Overall, our experiments revealed a defect in the amplitude of spontaneous Ca^{2+} events as well as significantly decreased Ca^{2+} responses when NMDAR-dependent synaptic plasticity was induced by glycine. This might arise from impaired ER Ca^{2+} handling via delayed and smaller ER Ca^{2+} release as well as an impaired refilling of Ca^{2+} into internal stores and increased SERCA-ATPase expression in NexCre cDKOs (see Fig. 7).

Re-expression of APPsα Rescues Impaired Ca^{2+} Handling and cLTP in NexCre cDKOs. Several previous studies demonstrated the neurotrophic function of the secreted APP ectodomain APPsα in synaptic plasticity (12, 45, 46). When APPsα was applied either as recombinant protein or introduced by virus-mediated expression,

it restored LTP deficits in NexCre cDKO mice (17, 39), aged wild-type (WT) rats (47), and in a mouse model of AD (38, 40). Based on these findings, we asked if providing APPsα to hippocampal neurons might have comparable effects on the observed defect in Ca^{2+} handling in NexCre cDKO neurons.

First, hippocampal cultures were preincubated with phosphate-buffered saline (PBS) or recombinant APPsα (recAPPsα, 10 nM) in Hanks' Balanced Salt Solution (HBSS). Subsequently, cLTP was induced while respective perfusion media circulated in a closed loop (Fig. 2*A*). Treating NexCre cDKO cultures with PBS revealed again a significant decrease in Fura2-AM/Ca^{2+} fluorescence of NexCre cDKO cells compared to LMs during spontaneous activity and impaired Ca^{2+} amplitude elevations upon cLTP induction [Fig. 2*B*, two-way RM ANOVA genotype, $F(1, 15) = 19.46$, $P = 0.0005$; post hoc Fisher's LSD, p(−20) = 0.002, p(−10) = 0.021, p(0) = 0.002, p(10) = 0.036, p(40) = 0.037]. Providing cDKO cultures with recAPPsα increased spontaneous fluorescence ratios under baseline conditions, although not significantly, whereas ratios were similar to PBS-treated NexCre cDKO cultures upon cLTP induction [Fig. 2*C*, two-way RM ANOVA time × genotype, $F(4, 84) = 2.014$, $P = 0.100$; post hoc Fisher's LSD, p(−20) = 0.012, p(−10) = 0.045]. Thus, recAPPsα treatment failed to enhance Ca^{2+} transients.

Recently, Mockett et al. (48) showed that APPsα is able to enhance GluA1 synthesis on a 30 min timescale, and we therefore asked if the content of Ca^{2+}-permeable GluA1 receptors might be enhanced upon recAPPsα perfusion (Fig. 2*D*). The overall density (Fig. 2*E*) and fluorescence intensity (Fig. 2*F*) of dendritic GluA1 puncta was not significantly different between genotypes or treatment. However, the density of synaptic GluA1 puncta, as assessed by the number of GluA1 puncta colocalized with synapsin, was reduced for NexCre cDKOs treated with PBS [Fig. 2 *D* and *G*, two-way ANOVA genotype, $F(1, 65) = 4.325$, $P = 0.042$; post hoc Fisher's LSD, p(NexCre) = 0.059]. In contrast, recAPPsα treatment of APP/APLP2-deficient neurons did not change GluA1 subunit levels nor restored Ca^{2+} transients, and therefore, a possible contribution of GluA1 in cLTP of Ca^{2+} transients cannot be excluded. In order to support our hypothesis that Ca^{2+}-permeable glutamate receptors are not involved or affected by recAPPsα treatment upon cLTP induction, we stained our cultures for GluA2 subunits and the presynaptic marker synapsin (Fig. 2 *H–J*). The treatment with recAPPsα increased GluA2 cluster density only in LMs [Fig. 2*H*, two-way ANOVA treatment, $F(1, 78) = 7.447$, $P = 0.008$; post hoc Fisher's LSD, p(LM) = 0.003], while the treatment decreased GluA2 cluster intensity in NexCre cDKOs compared to LMs treated similarly with the peptide [Fig. 2*I*, two-way ANOVA genotype, $F(1, 156) = 9.029$, $P = 0.003$; post hoc Fisher's LSD, p (APPsα) < 0.001]. This is in line with the publications of Borgdorff and Choquet (49) as well as Tardin et al. (50), which show that increased intracellular Ca^{2+} by glycine-induced stimulation regulates lateral diffusion of surface GluA2 between extrasynaptic and synaptic sites. Interestingly, recAPPsα treatment increased the synapsin cluster number in LM and NexCre cDKOs [Fig. 2*J*, two-way ANOVA treatment, $F(1, 78) = 13.65$, $P < 0.001$; post hoc Fisher's LSD, p(LM) = 0.009, p(NexCre) = 0.013], pointing toward a presynaptic effect of the extracellular APP domain supporting cLTP and intracellular Ca^{2+} increase.

As a next step, we aimed for a prolonged APPsα effect and transduced cultures 6 d before imaging with either the bicistronic AAV–APPsα vector, driving the expression of Venus and the codon-optimized HA-tagged murine, neurotrophic APPsα fragment, or a monocistronic AAV-Venus control vector, driving the expression of the membrane-anchored fluorescent protein Venus, as acute application failed to restore Ca^{2+} transients. The synapsin promotor ensured expression of APPsα and Venus specifically in neurons with a high transduction efficiency (Fig. 3 *A*, *Right*) (38, 39).

As shown before, cLTP induction increased Ca^{2+} amplitudes relative to spontaneous Ca^{2+} transients at baseline activity for both genotypes and irrespective of viral vector [Fig. 3*A*, two-way RM ANOVA time, $F(3{,}441, 210.8) = 51.57$, $P < 0.001$; Tukey's post hoc test]. Consistent with experiments without AAVs (Figs. 1 and 2), we observed significantly smaller amplitudes of spontaneous Ca^{2+} transients (baseline activity at t−20 and t−10) in NexCre cDKO cultures compared to LMs transduced with the AAV-Venus control vector [Fig. 3*B*, two-way RM ANOVA genotype, $F(1, 31) = 11.08$, $P = 0.002$; post hoc Fisher's LSD, p(t−20) = 0.013, p(t−10) = 0.012]. Furthermore, we detected significantly smaller Fura2-AM ratios upon cLTP induction in NexCre cDKO neurons compared to LM neurons expressing Venus [Fig. 3*B*, two-way RM ANOVA genotype, $F(1, 31) = 11.08$, $P = 0.002$; post hoc Fisher's LSD, p(t10) = 0.005, p(t40) = 0.003]. Interestingly, AAV-driven re-expression of APPsα rescued the significantly reduced Ca^{2+} amplitudes not only under baseline conditions [Fig. 3*B*', two-way RM ANOVA treatment, $F(1, 31) = 11.16$, $P = 0.002$; post hoc Fisher's LSD, p(t−20) = 0.014, p(t−10) = 0.002] but notably also upon cLTP [Fig. 3*B*', two-way RM ANOVA treatment, $F(1, 31) = 11.16$, $P = 0.002$; post hoc Fisher's LSD, p(t0) = 0.008, p(t10) = 0.073, p(t40) = 0.007] in NexCre cDKO cultures. Thus, our experiments confirm the crucial role of APPsα in synaptic plasticity by its ability to rescue cLTP in NexCre cDKO cultures upon prolonged APPsα re-expression. As the acute application of recAPPsα had only minor effects on Ca^{2+} handling in NexCre cDKOs, this clearly indicates that APPsα affects protein expression rather than enhancing Ca^{2+} channel function.

APPsα Restores Up-Regulated SERCA-ATPase Activity by Regulating Its Expression Level. Next, we compared cLTP responses in APPsα re-expressing cells when the SERCA-ATPase was blocked by CPA. We were interested whether AAV–APPsα might restore normal ER Ca^{2+} signaling in NexCre cDKO neurons (compared to data shown in Fig. 1 *C* and *C*').

Re-expressing APPsα in LM cultures led to a strongly impaired glycine-induced Ca^{2+} rise when the SERCA-ATPase was blocked during cLTP induction [Fig. 4*A*, two-way RM ANOVA time, $F(2.443, 83.06) = 51.03$, $P < 0.001$; Tukey's post hoc test] compared to t0 p(t−10) = 0.029, p(t10) = 0.031, p(t40) = 0.001). This effect size is comparable to LM cultures that were transduced with AAV-Venus [Fig. 4*A*, Tukey's post hoc test, compared to t0 p(t−20) = 0.041, p(t−10) = 0.003, p(t10) = 0.035, p(t40) = 0.006]. In contrast, NexCre cDKO cultures expressing only Venus showed a highly significant increase in intracellular [Ca^{2+}] both at t0 and t10 as described before (Fig. 1 *C* and *C*'), which decreased at t40 upon the complete washout of the reversible CPA blocker [Fig. 4*A*, Tukey's post hoc test, compared to t0 p(t−20) < 0.001, p(t−10) < 0.001, compared to t10 p(t−20) = 0.017, p(t−10) = 0.042]. Consistently, NexCre cDKO cultures transduced with AAV-Venus revealed the same phenotype of impaired ER Ca^{2+} handling as seen without viral vectors [Fig. 4*A*, Tukey's post hoc test, compared to t0 p(t−20) = 0.047, p(t−10) = 0.022, p(t10) = 0.012, p(t40) = 0.002], further corroborating the altered function of the ER loading ATPase. This is even more evident when comparing normalized Ca^{2+} ratios at single-imaging time points (Fig. 4*A*'). We additionally detected a strong rise in intracellular [Ca^{2+}] specifically in NexCre cDKO transduced with the AAV-Venus following cLTP stimulation and CPA treatment at t0, t10, and t40. This also confirmed the previous observation of impaired ER Ca^{2+} handling in APP/APLP2-deficient neurons [Fig. 4*A*', two-way RM ANOVA time × genotype, $F(9, 102) = 6.445$, $P < 0.001$; Tukey's post hoc test, compared to NexCre Venus at t0 p(LM Venus) = 0.004, p(LM APPsα) = 0.004, p(NexCre APPsα) = 0.005, compared to NexCre Venus at t10 p(LM Venus) = 0.012, p(LM APPsα) = 0.009, p(NexCre APPsα) = 0.031, compared to NexCre Venus at t40 p(LM Venus) = 0.047, p(LM APPsα) = 0.044].

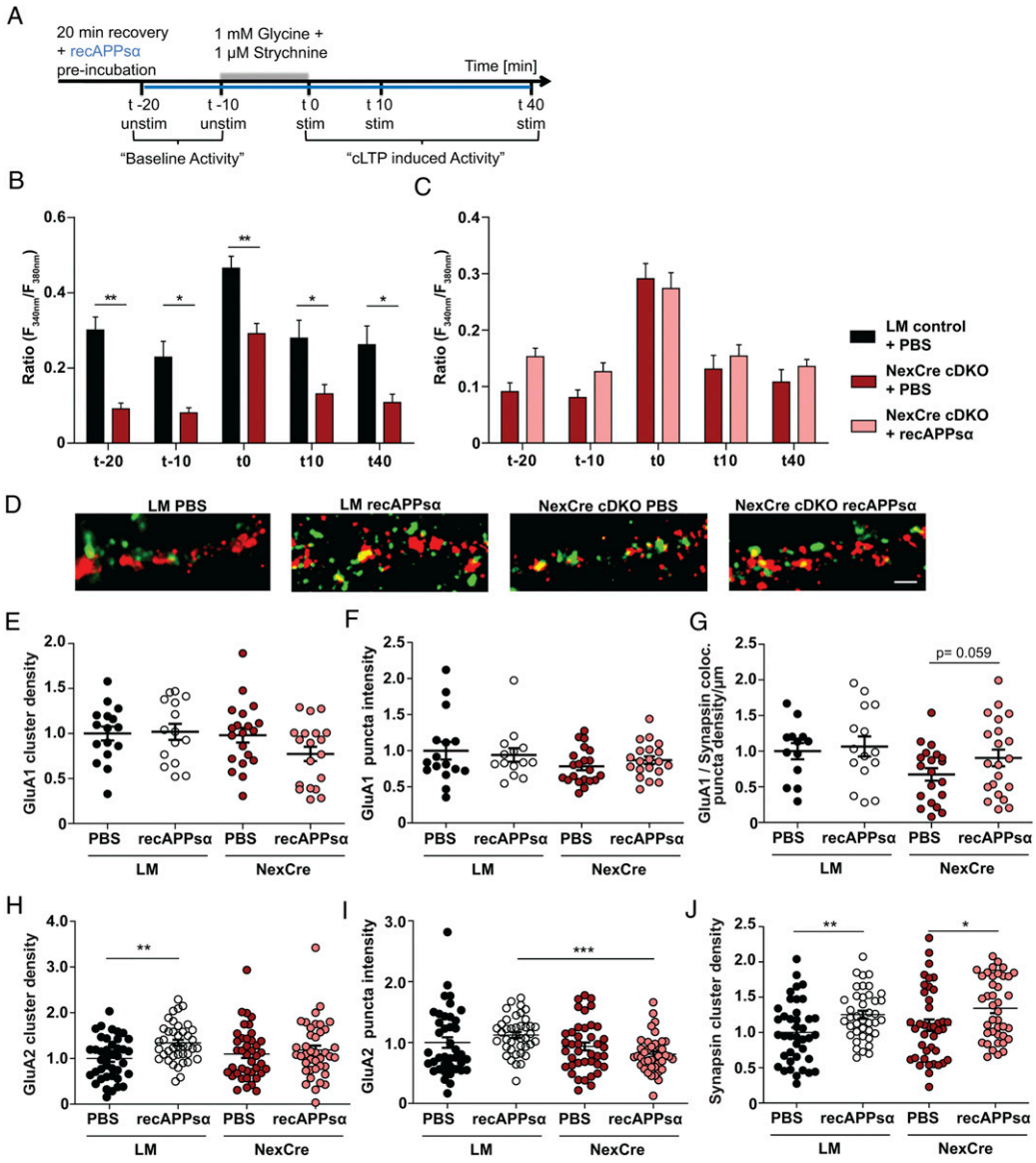

Fig. 2. Acute APPsα treatment elevates cytosolic Ca^{2+} amplitudes but fails during cLTP induction. (*A*) During 20 min of adaptation to chamber conditions, cultures were preincubated with PBS or recAPPsα (10 nM) in HBSS (t−20 and t−10). After the recording of "baseline activity," cLTP was induced by glycine and strychnine (t0) and subsequently washed out (t10 and t40). The perfusion solution circulated during the imaging procedure in a closed loop. (*B*) Imaging time points t−20 and t−10 mirror significant smaller relative changes in Fura2-AM/Ca^{2+} fluorescence when NexCre cDKO (n = 11/N = 4) cells were spontaneously active under PBS treatment compared to LMs (n = 6/N = 4). The quantified cytosolic Ca^{2+} changes upon glycine/strychnine application at t0, t10, and t40 were impaired in NexCre cDKOs perfused with PBS. (*C*) recAPPsα increased only in spontaneous Fura2-AM/Ca^{2+} fluorescence changes in NexCre cDKOs (n = 12/N = 4), while upon cLTP induction ratios were similar to PBS-treated cultures. (*D*) Cultures were stained for surface GluA1 receptors and synapsin. For illustration, all images were equally increased in brightness and contrast by the same absolute values. (Scale bar, 2 µm.) (*E*–*G*) Live-cell labeling of surface GluA1 receptors in LM controls and NexCre cDKOs upon PBS (LM n = 16/N = 3; NexCre cDKOs n = 20/N = 3) or recAPPsα treatment (LM n = 15/N = 3; NexCre cDKOo n = 19/N = 3) and cLTP. Normalized values for the cluster density (*E*), fluorescence intensity (*F*), and colocalization of GluA1 clusters and synapsin$^+$ puncta (*G*). (*H*–*J*) Live-cell labeling of surface GluA2 receptors in LM controls and NexCre cDKOs upon PBS or recAPPsα treatment and cLTP (n = 40/N = 3). recAPPsα treatment increased GluA2 cluster density in littermates (*H*), while the treatment decreased GluA2 fluorescence intensity in NexCre cDKOs compared to LMs treated similarly (*I*). recAPPsα treatment increased synapsin number per microliter in NexCre cDKOs and LMs (*J*). Values represent means ± SEMs, n = number of dendrites, N = independent number of culture preparations, significances were plotted as *P < 0.05, **P < 0.01, and ***P < 0.001.

Interestingly, NexCre cDKO neurons re-expressing APPsα behaved like LM cells transduced with either AAV-Venus or AAV–APPsα (Fig. 4*A*'). Thus, APPsα is able to restore altered ER Ca^{2+} handling in APP/APLP2-deficient neurons. These results could be due to an APPsα–mediated normalization of SERCA2 ATPase expression levels in NexCre cDKOs. We therefore quantified SERCA2 ATPase immunofluorescence (Fig. 4 *B*–*D*). And indeed, the results indicated a nearly 10-fold increase in the area covered by the somata of NexCre cDKOs compared to LM AAV-Venus–treated cultures [Fig. 4 *B* and *C*, two-way ANOVA genotype, $F(1, 24) = 59.12$, $P < 0.001$; post hoc Fisher's LSD, p(Venus) < 0.001]. Upon APPsα re-expression in APP/APLP2-deficient cultures, the area covered by the SERCA2 ATPase-positive somata in NexCre cDKOs was reduced to LM Venus control levels [Fig. 4 *B* and *C*, two-way ANOVA treatment, $F(1, 24) = 21.32$, $P < 0.001$; post hoc Fisher's LSD, p(NexCre) < 0.001]. Moreover, this significant effect can be observed not only between both genotypes [Fig. 4 *B* and *D*, two-way ANOVA genotype, $F(1, 24) = 13.65$,

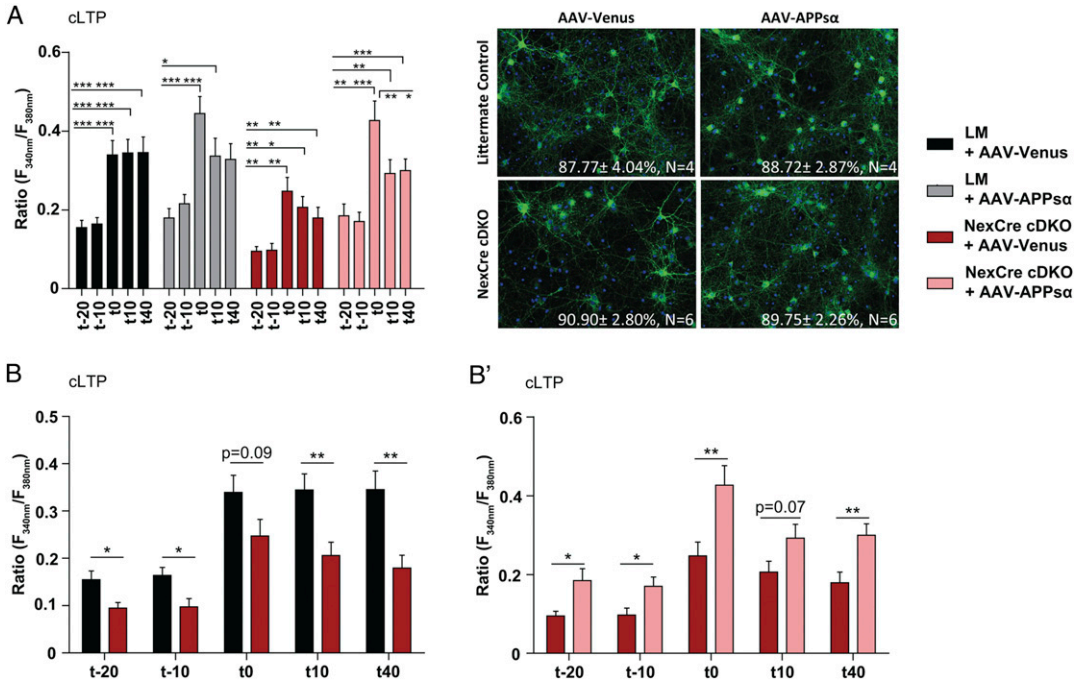

Fig. 3. Re-expression of APPsα rescues disturbed Ca^{2+} handling and impaired cLTP in NexCre cDKOs. (*A*) Imaging time points t−20 and t−10 mirror relative changes in Fura2-AM/Ca^{2+} fluorescence when cells were spontaneously active, while t0, t10, and t40 reflect quantified cytosolic Ca^{2+} changes upon cLTP induction by glycine and strychnine application. (*Left*) Upon glycine/ strychnine stimulation, LM controls transduced with AAV-Venus (black bars) showed a strong increase in relative cytosolic Ca^{2+} levels at t0, t10, and t40, while LM controls re-expressing APPsα (gray bars) failed to reach significant elevation in cytosolic Ca^{2+} amplitudes at t40. NexCre cDKO cultures treated with control virus (red bars) yielded a significant Ca^{2+} increase but to a lower extent that was not stable till t40. Ca^{2+} levels were significantly higher following APPsα re-expression in NexCre cDKOs (light red bars). (*Right*) Representative images of LM control or NexCre cDKO primary neuronal cultures transduced with AAV-Venus (LM n = 16/N = 7; NexCre cDKOs n = 17/N = 6) or AAV–APPsα (LM n = 17/N = 7; NexCre cDKOs n = 16/N = 6). The displayed values represent transduction efficiency. For illustration, all images were equally increased in brightness and contrast by the same absolute values. (*B*) Depicting both genotypes transduced with AAV-Venus revealed a significant reduction in basal Ca^{2+} amplitudes in NexCre cDKOs (red bars). Lowered relative Ca^{2+} levels were sustained upon glycine/stychnine administration by trend at t0 and significantly at t10 and t40. (*B'*) Illustration of the APPsα re-expression in NexCre cDKO cultures (light red bars) compared to NexCre cDKOs treated with AAV-Venus (red bars) showed that Ca^{2+} amplitudes at rest (t−20 and t−10) and upon cLTP induction were restored beside tendency at t10. Significances were plotted as $*P < 0.05$, $**P < 0.01$, and $***P < 0.001$. Error bars indicate ± SEM, n = number of cultures, N = independent number of culture preparations.

$P = 0.001$; post hoc Fisher's LSD, p(Venus) = 0.002] and within NexCre cDKOs [Fig. 4 *B* and *D*, two-way ANOVA treatment, $F(1, 24) = 8.38$, $P = 0.008$; post hoc Fisher's LSD, p(NexCre) = 0.005] for area but also for fluorescence intensity of SERCA2-positive somata. Overall, these data indicate that APPsα is essential for proper SERCA-ATPase activity by regulating its expression level. Furthermore, we studied ER Ca^{2+} dynamics following viral transduction using the ER–GCaMP6-150 Ca^{2+} indicator (Fig. 4 *E–H*). Notably, viral transduction altered ER Ca^{2+} behavior in both genotypes as shown in *SI Appendix*, Fig. S2 *D* and *E*. Comparing only virus transduced cultures revealed, first of all, that APPsα re-expression decreased the ER [Ca^{2+}] after 5 min CPA treatment in the last minutes of ER Ca^{2+} dynamic recordings [Fig. 4*E*, two-way RM ANOVA treatment, $F(1, 67{,}500) = 2{,}026$, $P < 0.0001$; post hoc Fisher's LSD, p(40 to 45 min) < 0.05]. Consistently to what we observed in the naïve situation, NexCre cDKO-Venus neurons showed an impaired refill of the ER Ca^{2+} pool and decreased ER [Ca^{2+}] upon 5 min CPA wash in [Fig. 4*F*, two-way RM ANOVA time × genotype, $F(2{,}699, 40{,}485) = 3.448$, $P < 0.0001$; post hoc Fisher's LSD, p(26 to 38 min) < 0.05]. Lastly, we detected that re-expression of APPsα in cDKO neurons neither changed ER Ca^{2+} dynamics when compared to viral transduced NexCre cDKO neurons with AAV-Venus (Fig. 4*G*) nor in LMs transduced with APPsα after 5 min CPA treatment (Fig. 4*H*). Overall, we conclude from these data, that APPsα re-expression enhances cytosolic [Ca^{2+}] by reducing the refill of the ER Ca^{2+} pool.

Reduced Spontaneous Ca^{2+} Dynamics in NexCre cDKO Cultures. Following a drop of ER [Ca^{2+}], for example, upon cLTP induction, this decrease is sensed by stromal interaction molecule 1 (Stim1) to refill ER stores directly via store-operated Ca^{2+} entry (SOCC) from the extracellular space (51, 52). This mechanism might be altered in APP/APLP2-deficient neurons, and therefore, we further studied whether APP/APLP2 has an influence also on this route of Ca^{2+} entry. To this end, we investigated spontaneous Ca^{2+} activity in NexCre cDKO cultures transduced with AAV–APPsα or AAV-Venus as well as in WT neurons (Fig. 5*A*). WT neurons were included in this analysis to compare changes in Ca^{2+} dynamics of the cDKO neuronal cultures as a control and to quantify the effect of AAVs when extracellular [Ca^{2+}] is altered. Following Ca^{2+} deprivation, WT cultures show a significant rise in the amplitude of spontaneous Ca^{2+} transients (t2 to t3) [Fig. 5*B*, two-way RM ANOVA time × genotype, $F(8, 172) = 3.529$, $P < 0.001$; Tukey's post hoc test, WT p(t2 to t3) = 0.014]. In order to examine the contribution of ER Ca^{2+} stores, we depleted these stores by coadministration of the SERCA-ATPase blocker CPA (10 μM) via perfusion of cells with HBSS containing a low Ca^{2+} concentration (Fig. 5*A*, t4). Monitoring spontaneous Ca^{2+} signals under these conditions revealed a reduction in the amplitude of spontaneous Ca^{2+} transients in WTs [Fig. 5*B*, Tukey's post hoc test, WT p(t3 to t4) = 0.011]. Subsequently, we monitored the SOCC-dependent Ca^{2+} entry by quantifying the amplitude of Ca^{2+} transients when external Ca^{2+} was restored, whereas the SERCA-ATPase was still blocked (Fig. 5*A*, t5) (25, 53). Under these

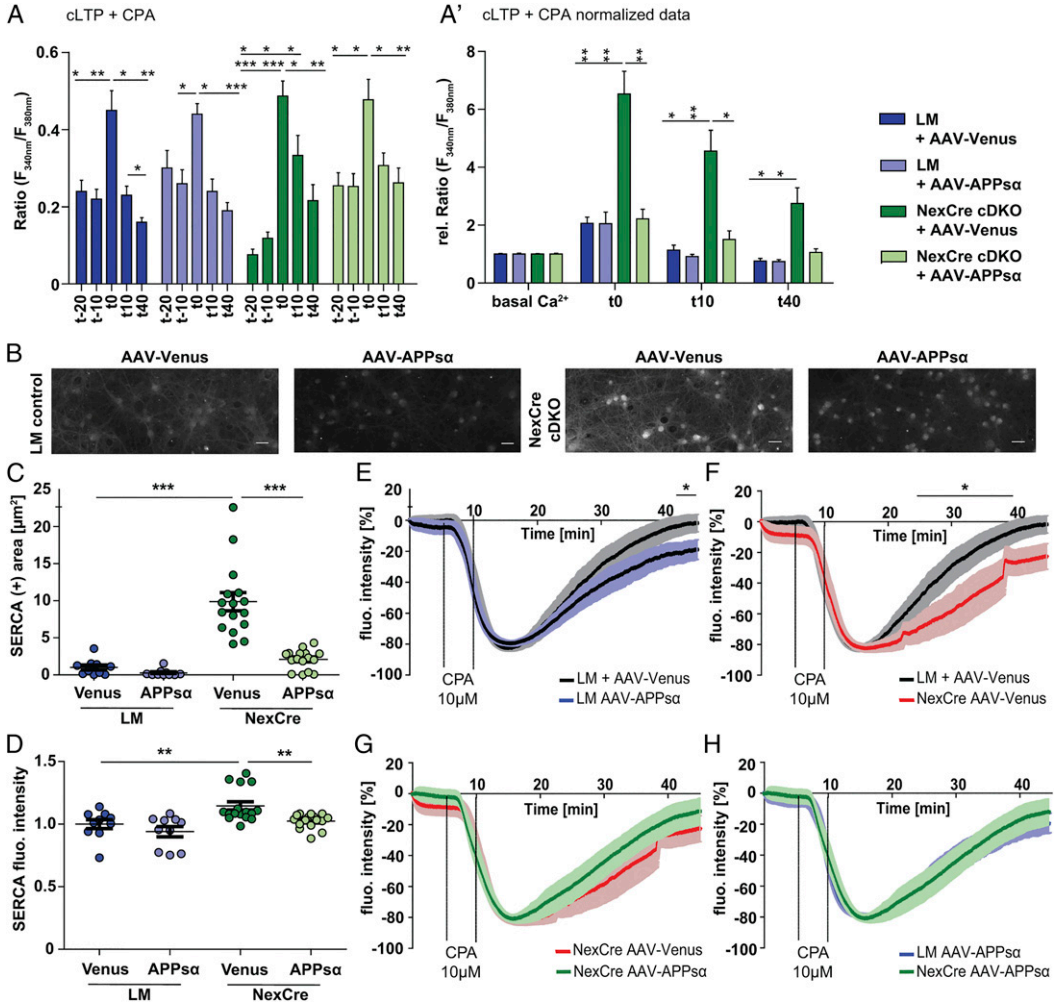

Fig. 4. Blocking of the ER-SERCA-ATPase elevates cLTP in NexCre cDKO cultures. Imaging time points t−20 and t−10 mirror relative changes in Fura2-AM/Ca^{2+} fluorescence when cells were spontaneously active, while t0, t10, and t40 reflect the quantified cytosolic Ca^{2+} amount upon cLTP induction by glycine and strychnine and/or CPA application. (*A* and *A'*) Blocking SERCA-ATPase activity during cLTP induction resulted in a significant increase in cytosolic Ca^{2+} levels in LM controls treated with AAV-Venus (blue bars; $n = 9/N = 4$), AAV–APPsα (light blue bars; $n = 9/N = 4$) and NexCre cDKOs re-expressing APPsα (light green bars; $n = 10/N = 3$) at t0, while no maintenance of relative Ca^{2+} level elevation was observable. NexCre cDKO cultures transduced with AAV-Venus (green bars; $n = 10/N = 3$) showed a highly significant increase in relative cytosolic Ca^{2+} levels at t0 and t10 and only a decrease at t40 (*A*). Comparing normalized Fura2-AM/Ca^{2+} ratios between genotypes at single-imaging time points demonstrated the powerful Ca^{2+} increase in NexCre cDKOs transduced with AAV-Venus following cLTP and CPA stimulation at t0, t10, and t40 (*A'*). (*B–D*) Representative images of anti-SERCA2 ATPase immunofluorescence for LM controls and NexCre cDKOs transduced either with AVV-Venus or AVV–APPsα. For illustration, all images were equally increased in brightness and contrast by the same absolute values. (Scale bar, 25 µm.) (*B*) anti-SERCA2 ATPase fluorescence signal quantified somatic area (*C*) and normalized mean fluorescence intensity of the protein (*D*). (*E–H*) Fluorescence intensity of ER-GCaMP6-150 transfected neuron upon 5 min CPA treatment. APPsα re-expression decreased the ER [Ca^{2+}] after 5 min CPA treatment in LM controls (AAV-Venus $n = 12$; AAV–APPsα $n = 15$) (*E*). NexCre cDKO-Venus ($n = 5$) neurons showed impaired refill of the ER Ca^{2+} pool and decreased ER [Ca^{2+}] upon 5 min CPA (*F*). Recording of NexCre cDKO ER-Ca^{2+} dynamics re-expressing APPsα ($n = 9$) was unaltered after 5 min CPA treatment compared to AAV-Venus (*G*) and LM AAV–APPsα (*H*). Significances were plotted as $*P < 0.05$, $**P < 0.01$, and $***P < 0.001$. Error bars indicate ± SEM, *n* = number of experiments, N = independent number of culture preparations.

conditions the [Ca^{2+}] recovered in WT neurons [Fig. 5*B*, Tukey's post hoc test, WT p(t4 to t5) = 0.014]. Analyzing NexCre cDKO neurons transduced with AAV-Venus (showed neither a significant change when reducing nor when increasing external [Ca^{2+}]. Monitoring the SOCC-dependent Ca^{2+} entry (t4 to t5) revealed that APP/APLP2-deficient neurons expressing AAV-Venus were not able to even partially increase intracellular [Ca^{2+}] as it has been observed for time point t2 to t3 [Fig. 5*B*, Tukey's post hoc test, NexCre Venus p(t3 to t5) = 0.007], indicating that SOCC-dependent Ca^{2+} entry is impaired in NexCre cDKO cultures.

Analyzing the behavior of mutant neurons that re-express APPsα revealed a significant reduction of Ca^{2+} ratios following external reduction in Ca^{2+} concentration (t1 to t2) that recovered completely after the readdition of external [Ca^{2+}] back to 3.8 mM (t3) [Fig. 5*B*, Tukey's post hoc test, NexCre APPsα p(t1 to t2) < 0.001, p(t2 to t3) = 0.011]. These data indicated that NexCre cDKO neurons re-expressing APPsα reveal a higher sensitivity to external Ca^{2+}, consistently to what is observed for WT cultures, and reflects Ca^{2+} entry via VGCCs, Ca^{2+} leakage from ER stores, and SOCC (see Fig. 7). Monitoring the SOCC-dependent Ca^{2+} entry revealed that APPsα re-expressing mutants can partially, but not significantly, increase intracellular [Ca^{2+}]. In conclusion, re-expressing APPsα appears to act via SERCA-ATPase, whereas it has little effect on impairing SOCC-dependent Ca^{2+} entry in NexCre cDKO cultures.

Additionally, VGCCs modulate the cytoplasmatic [Ca^{2+}]. Therefore, we performed the same set of experiments while blocking these Ca^{2+} channels using 10 µM nifedipine (Fig. 5*A*). Under the assumption that VGCCs will be targeted by APP or APLP2, we assessed the role of APPsα in changing [Ca^{2+}] after

Ca^{2+} wash out, and the readdition was imaged at time points t2 to t3 in NexCre cDKO. The previously detected increase in Ca^{2+} concentration at t2 to t3 was not detected in NexCre cDKO cultures transduced with APPsα [Fig. 5*C*, two-way RM ANOVA time × genotype, $F(8, 86) = 3.243$, $P = 0.003$; Tukey's post hoc test, NexCre APPsα p(t2 to t3) = 0.426]. Interestingly, nifedipine treatment enhanced Fura2-AM ratios in NexCre cDKOs transduced with the control virus (t1) as observed for cLTP induction in the naïve mutants when VGCCs were blocked (Fig. 5*C* and *SI Appendix*, Fig. S2 *B* and *C* compared to Fig. 5*B*), arguing for an increased Ca^{2+} leakage from ER stores and, as we could show in Fig. 5*B*, impaired Ca^{2+} entry via SOCC in NexCre cDOK neurons. Furthermore, APPsα seems to mediate the influx of Ca^{2+} via L-type VGCCs as APPsα–transfected neurons sense Ca^{2+} changes in Fig. 5*B* at t3 without applying nifedipine, while instead, nifedipine treatment prevented it at t3 in Fig. 5*C*. Monitoring lastly, the SOCC contribution to the amplitude of spontaneous Ca^{2+} transients (Fig. 5*C*, t4 to t5) revealed an impaired uptake of external Ca^{2+} for all experimental groups analyzed.

To gain further mechanistic insight into the mechanism how SOCC-dependent Ca^{2+} entry might be impaired, we examined the expression of ER-localized SOCC initiators Stim1 and Stim2, both highly expressed in the murine hippocampus (54, 55). Indeed, we found a strongly enhanced expression of Stim1 protein in the somata of APP/APLP2-deficient neurons transduced with the control vector (Fig. 5*D*). The measured area of Stim1 expressing NexCre cDKO AAV-Venus–transduced cells was about 40-fold higher than in LM controls [Fig. 5 *D* and *E*, two-way ANOVA genotype, $F(1, 51) = 102.1$, $P < 0.001$; post hoc Fisher's LSD, p(Venus) < 0.001] and decreased significantly upon APPsα treatment [Fig. 5 *D* and *E*, two-way ANOVA treatment, $F(1, 51) = 43.54$, $P < 0.001$; post hoc Fisher's LSD, p(NexCre) < 0.001]. Furthermore, this effect could also be observed in the fluorescence intensity of Stim1-positive somata between genotypes [Fig. 5 *D* and *F*, two-way ANOVA genotype, $F(1, 51) = 141.4$, $P < 0.001$; post hoc Fisher's LSD, p(Venus) < 0.001, p(APPsα) < 0.001] and within NexCre cDKO [Fig. 5 *D* and *F*, two-way ANOVA treatment, $F(1, 51) = 23.34$, $P < 0.001$; post hoc Fisher's LSD, p(NExCre) < 0.001]. Similar but less pronounced effects were observed for Stim2. The area of Stim2-positive somata in NexCre cDKO was significantly increased by fivefold of the LM control (Fig. 5*G*, unpaired *t* test, $P = 0.009$), while the fluorescence intensity of Stim2 showed no significant difference (Fig. 5*H*). Taken together, these data indicate that APP and APLP2 are essential for the accurate activity of SOCC and regulate the expression of Stim1 and 2, especially by the ectodomain APPsα.

Ex Vivo cLTP and Spontaneous Calcium Transients. Last, we wanted to confirm our data in a more in vivo–directed approach using acute hippocampal slices. To this end, we recorded *f*EPSP at the Schaffer collateral to the CA1 pathway and applied 10 mM glycine after a stable baseline recording of 20 min (Fig. 6*A*). LM control animals deficient for APLP2 showed unaltered *f*EPSP in comparison to WT C57Bl6 animals upon cLTP induction, which is in line to TBS-induced LTP (15). Interestingly, NexCre cDKOs show a trend toward increased *f*EPSP signals compared to LM controls [Fig. 6 *A* and *B*, one-way ANOVA, Tukey's post hoc test, p (85 to 90 min) = 0.08], while TBS-induced LTP is significantly reduced in slices of these animals (17). In contrast to TBS-induced LTP, which is based on the increased release of a neurotransmitter from the presynaptic terminal of CA3 axons, glycine only acts on postsynapticly expressed NMDA receptors. The trend of increased *f*EPSP signals of NexCre cDKOs might underline the modulatory role of presynaptic input additionally affected by APP family members.

Furthermore, we studied spontaneous Ca^{2+} transients of CA1 pyramidal neurons in acute hippocampal slices of LM control and NexCre cDKO animals originated from the same mice used for cLTP experiments. Using the Ca^{2+} indicator Fura2-AM, we adapted the protocol of Cameron et al. (56) and focused on the CA1 cell body layer (Fig. 6*C*). While we did not detect any significant difference in spontaneous Ca^{2+} signal frequency (Fig. 6*D*) and amplitude (Fig. 6*E*), still smaller spontaneous Ca^{2+} amplitudes were detected in slices of NexCre cDKO animals [ratio(LM) = 0.078 ± 0.026 versus ratio(NexCre) = 0.049 ± 0.014], mirroring results of Ca^{2+} dynamics in our culture system described at the beginning (Fig. 1).

Discussion

Neuronal Ca^{2+} signaling is fundamental for homeostatic and adaptive cell function, as it controls enzymatic signaling cascades up to gene transcription. Impairments in Ca^{2+} handling have been implicated in a variety of neurodegenerative diseases including AD (1–4, 34), as mutations within the genes causing familial AD increase intracellular [Ca^{2+}], for example, by the overloading of ER stores (30, 43, 57), altered SOCC entry (30, 32, 58), or enhanced influx through Aβ-formed cell membrane pores (33). In contrast to the well-studied dysregulation of Ca^{2+} homeostasis in AD, the physiological function of other APP cleavage peptides or APP family members received less attention with regard to their role in Ca^{2+} signaling.

In the present study, we identify a specific role for APP/APLP2 to support Ca^{2+} homeostasis and by this means, synaptic plasticity. NMDA receptor–dependent LTP induction resulted in a strong and prolonged increase in the amplitude of global Ca^{2+} transients in primary cultures consistent with observations in acute hippocampal slices (59) or organotypic cultures (60). Interestingly, Fura2-AM ratios upon cLTP induction were significantly reduced in APP/APLP2-deficient neurons, consistent with the previously described impaired LTP and STP (17, 39) in slice recordings of APP/APLP2 mutant mice. Of note, the induction of cLTP in acute slices resulted in the opposite phenomena; by trend enhancing *f*EPSP in NexCre cDKO compared to WTs and LM controls underlying the modulatory input of APP family proteins at presynapses. We reported recently that the acute application of recombinant APPsα increased the magnitude of LTP in cDKO slices (17), while AVV-mediated expression of APPsα in brains of cDKO restored not only LTP but in addition STP (39). Here, we provide evidence that altered Ca^{2+} signaling contributes to impaired activity-dependent synaptic plasticity in APP/APLP2 cDKOs by controlling the expression of central ER Ca^{2+} store proteins, the SERCA-ATPase, and SOCC-associated proteins Stim1 and 2. Moreover, we could identify that cDKO mutants show a trend toward the slower release of Ca^{2+} from ER Ca^{2+} stores and Ca^{2+} content while the refilling of Ca^{2+} was significantly impaired, explaining why spontaneous cytosolic Ca^{2+} amplitudes are significantly smaller in mutants. Moreover, we observed a pronounced increase in the abundance of SERCA2 ATPase, Stim1, and Stim2 proteins in the somata of APP/APLP2-deficient neurons, providing an additional explanation for functional impairments. Most notably, these alterations were normalized upon APPsα expression. In this respect, it is noteworthy that APP and Stims have similar transmembrane sequences, especially at the γ-secretase cleavage site (36, 58). Increased γ-secretase processing of Stims (58, 61) or excessive ER Ca^{2+} store filling might be the cause of attenuated SOCC activity, similar to what we observed in our APP/APLP2 cDKO cultures and how it was reported in PS1 knock-in mice (62). Moreover, SOCC-mediated Ca^{2+} entry was impaired in APP-KO astrocytes, including reduced expression of TRPC1 (C-type transient receptor potential) and Orai1 proteins, other essential SOCC components (25). In addition, our findings are also in line with the altered Stim1 and 2 expression shown in PS-deficient and APP knock-in cells as well as in sporadic AD patients and aged WT mice (30, 61, 63).

In this respect, it is remarkable that SOCC is important for processes of synaptic plasticity, as it regulates neurotransmitter

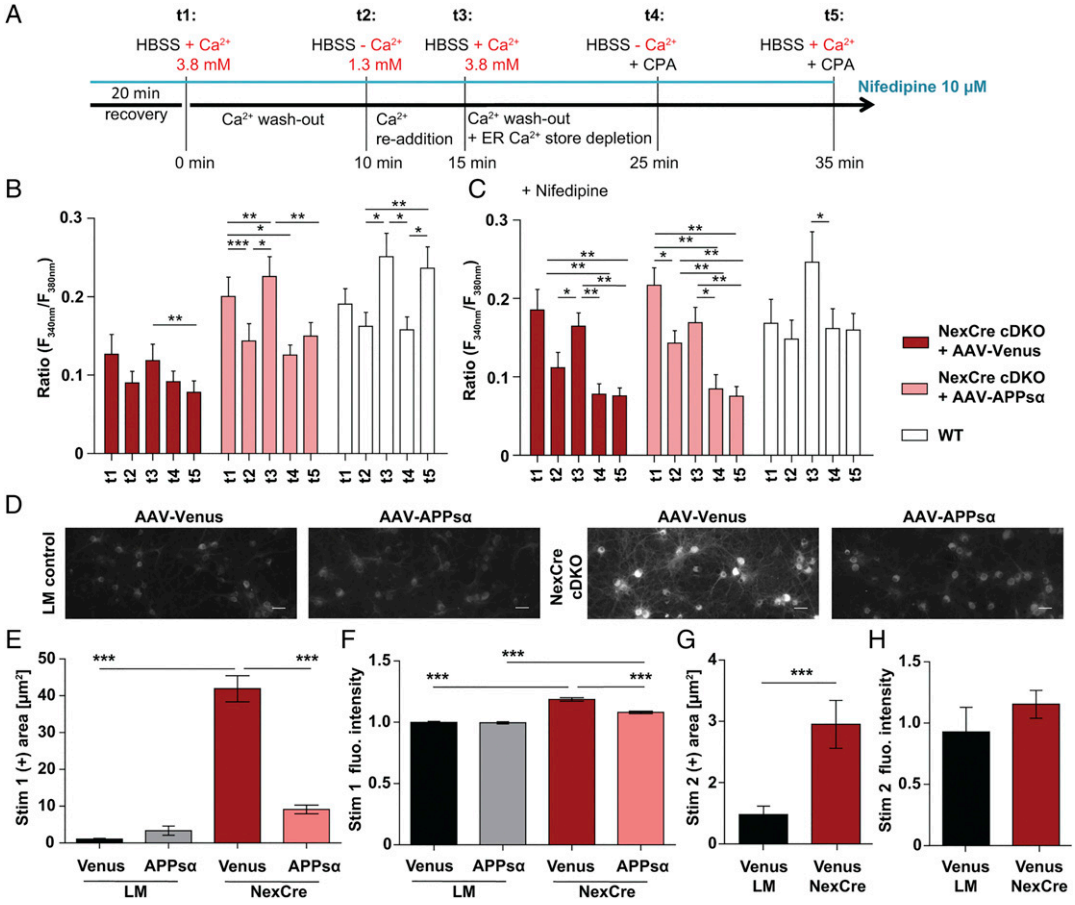

Fig. 5. Altered Ca^{2+} dynamic in NexCre cDKO cultures under basal conditions. (*A*) Experimental setup quantifying spontaneous Ca^{2+} activity (t1) following reduction of external [Ca^{2+}] to 1.3 mM (t2) and readdition of Ca^{2+} (t3, recovery). Lowering external [Ca^{2+}] to 1.3 mM and additionally ER Ca^{2+} depletion by CPA (t4) is shown. Subsequent restoration of external [Ca^{2+}] to 3.8 mM while blocking SERCA-ATPase monitoring SOCC-dependent Ca^{2+} influx (t5). With or without additional blockage of VGCCs using 10 µM Nifedipine (blue line). (*B*) Small decline in fluorescence ratios at spontaneous activity in NexCre cDKOs+AAV-Venus (red bars, $n = 15/N = 5$) upon reduction of external Ca^{2+} (t1 to t2) that was partially restored when external [Ca^{2+}] was increased (t2 to t3). No SOCC-dependent Ca^{2+} entry in NexCre cDKOs transduced with AAV-Venus (t4 to t5). AAV–APPsα–treated cDKO cultures (light red bars, $n = 15/N = 5$) revealed a decrease in the amplitude of Ca^{2+} transients at spontaneous activity following the reduction of external Ca^{2+} (t1 to t2) and full recovery of relative Ca^{2+} amounts when external Ca^{2+} was restored (t2 to t3) comparably to WTs (white bars, $n = 15/N = 6$). Small, but detectable SOCC-dependent Ca^{2+} entry in NexCre cDKOs+AAV-APPsα cultures at spontaneous cell activity (t4 to t5) that is obvious in WTs (t4 to t5). (*C*) Significant reduction in fluorescence ratios at spontaneous activity upon reduction of external [Ca^{2+}] to 1.3 mM (t1 to t2) in all groups and only partial recovery when external Ca^{2+} was restored (t2 to t3) in AAV-transduced NexCre cDKOs (red and light red bars; AAV-Venus $n = 10/N = 3$; AAV–APPsα $n = 10/N = 3$) and completely in WTs (white bars, $n = 5/N = 3$). No SOCC-dependent Ca^{2+} entry when VGCCs were blocked in all groups (t4 to t5). (*D–F*) Representative images of Anti-Stim1 immunofluorescence for LM controls and NexCre cDKOs transduced either with AVV-Venus or AVV–APPsα. For illustration, all images were equally increased in brightness and contrast by the same absolute values. (Scale bar, 25 µm.) (*D*) Quantified somatic area of Stim1 (*E*) and normalized mean fluorescence intensity (*F*). (*G* and *H*) Immunofluorescence of the Stim2 protein in naïve cultures is depicted and quantified for somatic area (*G*) and mean fluorescence intensity (*H*) upon respective virus transduction. Significances were plotted as $*P < 0.05$, $**P < 0.01$, and $***P < 0.001$. Error bars indicate ± SEM, *n* = number of experiments, N = independent number of culture preparations.

release and refills ER Ca^{2+} stores during neurotransmission (51, 53), processes that are impaired in NexCre cDKO neurons (17, 39). The examination of SOCC-dependent Ca^{2+} entry (25, 53) revealed that only NexCre cDKO cells expressing APPsα displayed Ca^{2+} influx via SOCCs, while cDKOs treated with the control vector failed to enhance the amplitude in baseline Ca^{2+} transients. NexCre cDKO cultures showed even a small decline in the amplitude of Ca^{2+} transients during spontaneous activity, indicating that the SOCC-dependent Ca^{2+} entry might be impaired upon APP and APLP2 deletion. Consistently, Copanaki, et al. (64) reported an APP-dependent amplification of SOCC entry after store depletion in PC12 cells. However, it needs to be taken into account that changes in Ca^{2+} dynamics occur on a very rapid timescale in neurons and are regulated by a variety of channels (11).

SOCC is initiated by ER Ca^{2+} depletion, for example, during LTP induction, in which NexCre cDKO neurons showed significantly decreased Ca^{2+} responses due to impaired ER Ca^{2+} handling. We could rescue this alteration functionally by CPA application, which leads to increased SERCA-ATPase levels in NexCre cDKO neurons. Importantly, both impaired SERCA activity and expression were rescued upon APPsα re-expression in APP/APLP2-deficient cultures, establishing the APPsα fragment as an important regulator of ER Ca^{2+} handling. Increased SERCA activity implies increased ER Ca^{2+} loading as observed for APP/APLP2 mutants and also well known to be influenced by Aβ (65, 66), PS (9), and the APP intracellular domain (24, 27). Knockdown of only APP in T84 cells by RNA interference did not affect the abundance of SERCA2, STIM1, or Orai1 proteins but elevated resting [Ca^{2+}] in the ER and lowered ER Ca^{2+} leakage rates (11). We found that the SOCC components Stim1 and 2 were up-regulated in double mutants lacking both APP and APLP2. This argues for a complementary role of APLP2 in Ca^{2+} regulation. Further, dysregulated Ca^{2+} signaling has previously been observed in APP-deficient astrocytes (25), cortical

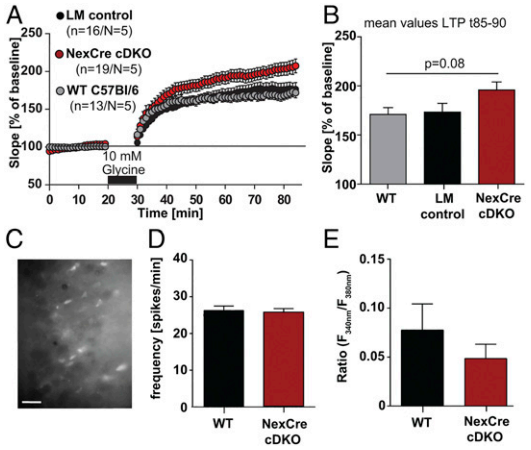

Fig. 6. Ex vivo cLTP measured by *f*EPSP at CA3-CA1 synapses and spontaneous Ca^{2+} transients of CA1 pyramidal neurons. (*A* and *B*) Trend toward increased *f*EPSP signals in NexCre cDKOs compared to LM controls. LM control animals deficient for APLP2 showed unaltered *f*EPSP in comparison to WT C57Bl6 animals upon cLTP induction (*A*). Mean values of 85 to 90 min after cLTP show no significant differences between the genotypes (*B*). (*C–E*) Representative image of Fura2-AM–labeled neurons of CA1 pyramidal neurons in acute hippocampal slice (*C*). No significant difference in spontaneous Ca^{2+} signal frequency (*D*) and amplitude (*E*) of analyzed spontaneous Ca^{2+} transients. The spontaneous Ca^{2+} amplitudes in slices of NexCre cDKO animals (n = 14/N = 3, 25 spots) was slightly smaller compared to LM controls (n = 14/N = 3, 21 spots). n = number of experiments, N = independent number of culture preparations

neurons with APP knockdown (67), and using CTb cells derived from a mouse model of murine Down syndrome (68). Overall, these observations and our own data reported here indicate that APP and APLP2 are necessary to control especially ER Ca^{2+} content as either APP/APLP deletion or APP overexpression lead to its dysregulation. We found strong evidence that APPsα serves as the crucial functional domain, supporting our previous findings in which recAPPsα application and AAV-mediated APPsα expression enhanced synaptic plasticity (17, 39). In the current study, APPsα rescued the cLTP deficit and moreover also impaired Ca^{2+} handling during baseline activity but only following prolonged expression. An acute application of recombinant APPsα enhanced solely the amplitude of baseline Ca^{2+} transients in NexCre cDKO neurons but failed to restore Ca^{2+} amplitudes to the LM control level upon cLTP. We investigated if this baseline increase in Ca^{2+} amplitudes of recAPPsα was attributable to an up-regulation of Ca^{2+}-permeable GluA1 receptors as shown by Mockett et al. (48) and observed a slight but not significant reduction in synaptic GluA1 clusters in APP/APLP2-deficient neurons that was prevented in the presence of recAPPsα. However, a significant increase was found for GluA2 clusters, which support the maintenance of LTP, upon APPsα treatment in littermates, while the treatment only reduced GluA2 cluster intensity in cDKOs treated similarly with the peptide. As we detected no alterations in cDKOs treated with PBS in the AMPA receptor subunit cluster analysis, we conclude that those receptors are not responsible for impairments in Ca^{2+} amplitudes and instead other Ca^{2+} permeable channels were modulated by APPsα, for example, VGCCs. Interestingly, recAPPsα increased the synapsin cluster number in NexCre cDKOs and LMs, pointing toward a modulatory presynaptic role of the extracellular APP domain. Blocking VGCCs did not result in differences in the amplitude of Ca^{2+} transients between cDKO cells with or without APPsα when extracellular [Ca^{2+}] in the perfusion medium was first reduced and then restored. These results show that the additional increase upon external Ca^{2+} reconstitution observed in cells expressing APPsα following viral transduction might be mediated in parts by enhanced VGCC function most likely via APPsα. In earlier studies, it has been shown that the expression of Cav1.2 L-type VGCC channels is up-regulated by Aβ formation (69), and its blockage has been identified as a potential pharmacotherapeutic target for AD (70, 71). APPsα contains the N-terminal residues of Aβ, which might alter Cav1.2 function. Moreover, it was shown that APP modulates Cav1.2 channels in cultured striatal and hippocampal GABAergic neurons (72) and rat primary cortical neurons (67). Recently, Hefter et al. (73) reported a neuroprotective role of APP, especially APPsα, with regard to altered VGCC action in response to hypoxia. Overall, a balanced activity of Ca^{2+} channels to maintain Ca^{2+} homeostasis is fundamental for neuronal function, and there is evidence that it is regulated by APP/APLP2 and their diverse proteolytic fragments. In this regard, the APPsα fragment produced by nonamyloidogenic processing is mediating neuroprotective and neurotrophic effects, whereas the amyloidogenic cleavage product Aβ is detrimental. This in turn implicates that a shift in APP cleavage toward amyloidogenic processing disturbs this balance and causes a loss of neuroprotective functions, which may contribute to disease development (74).

Taken together, we were able to show that altered Ca^{2+} signaling is linked to impaired Ca^{2+} homeostasis in the absence of APP/APLP2 (Fig. 7). We demonstrate that APP and APLP2 are essential to maintain intracellular [Ca^{2+}] during spontaneous activity. Impairments in the absence of both proteins are the result of a disturbed SERCA-ATPase activity at ER Ca^{2+} stores and the release from as well as refill of Ca^{2+} into those stores. Furthermore, the function of VGCC and SOCC is modulated by APP/APLPs. APP/APLP2 deficiency led to significantly smaller Ca^{2+} transients upon induction of LTP. Most importantly, we show that all reported impairments in APP/APLP2 cDKO neurons can be mainly attributed to the lack of the neurotrophic APPsα domain as APPsα re-expression rescued Ca^{2+} homeostasis as well as LTP. In line with this, APPsα is able to modulate ER Ca^{2+} store refilling, VGCC and SOCC channel function, highlighting its neurotrophic action as a crucial functional domain and strengthening its therapeutic potential with regard to altered Ca^{2+} homeostasis in AD.

Materials and Methods

Mice/Cell Culture. The primary cultures of mouse hippocampal neurons were prepared using $NexCre^{+/T}$ $APP^{flox/flox}APLP2^{-/-}$ (NexCre cDKO) and $APP^{flox/flox}APLP2^{-/-}$ LM mice at embryonic day 18.5. The generation and genotyping of APP conditional mice is described in detail by Hick et al. (17). C57Bl6 mice were used in control experiments. All procedures concerning animals were approved by the animal welfare representative of the Technische Universität Braunschweig and the Lower Saxony State Office for Consumer Protection and Food Safety [Oldenburg, Germany, Az. §4 (02.05) TSchB Technische Universität Braunschweig].

AAV Constructs and Transduction of Primary Cultures. The AAV constructs AAV–APPsα and AAV-Venus have been described [Fol et al. (38), Richter et al. (39)]. AAV-Venus and AAV–APPsα were added to primary hippocampal cultures of NexCre cDKO or littermate control mice 6 d before imaging at a multiplicity of infection (MOI) of 2×10^4.

Ca^{2+} Imaging Experiments.

Fura2-AM. Ca^{2+} imaging experiments were performed with cultured hippocampal neurons at DIV12 to DIV16. The loading of neuronal cultures was done with 4 mM Fura2-AM (Life Technologies, solved in dimethyl sulfoxide) solved in HBSS with 2.5% Pluronic F127 (Sigma) for 45 min at 37 °C. For time lapse imaging taking 500 images in a cycle time of 326 ms and 200 cycles repetition, the light intensity was set to 70.9%, and the exposure time was kept constantly at 130 ms.

cLTP induction. Following 20 min of adaptation to chamber conditions, two images of spontaneous activity (baseline activity) were taken at an interval of 10 min (t–20, t–10). A 10-min bath application of 1× HBBS containing glycine (1 mM) and strychnine hydrochloride (1 μM, Sigma), blocking specifically endogenously expressed glycine receptors, was used for stimulation and cLTP induction followed by continuous perfusion with 1× HBBS to acquire three additional time

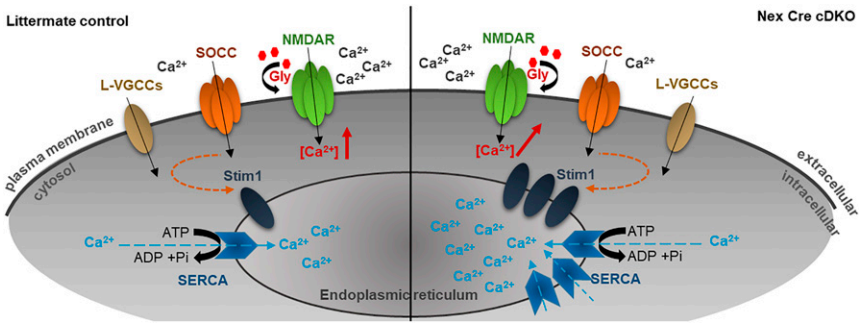

Fig. 7. APP and APLP2 are essential regulators of Ca^{2+} homeostasis, a mechanistic inside. Depicted is a model of how and why hippocampal neurons of cDKO mice (*Right*) might have lower intracellular [Ca^{2+}] in comparison to littermates (*Left*) during spontaneous neuronal activity. Smaller Ca^{2+} amplitudes are likely attributable to compartmentalized Ca^{2+} in ER Ca^{2+} stores due to increased SERCA-ATPase and Stim1 and Stim2 expression, which alters the refilling of Ca^{2+} in APP/APLP2-deficient neurons. LTP induction results in a significant rise in Ca^{2+} amplitudes only in littermate controls, while cDKOs show impairments in LTP induction and maintenance to the same extent. This defect in synaptic plasticity is most likely due to disturbed SERCA-ATPase activity at ER Ca^{2+} stores upon APP and APLP2 deletion as increased ATPase expression will lead to an increase in Ca^{2+} transport into the ER.

points upon cLTP induction (t0, t10, and t40). In additional experimental settings, we coadded CPA (10 μM, Tocris) or nifedipine (10 μM, Tocris) (75).

ER-camp-150 experiments. Naïve cultures as well as neuronal cultures transduced before with AAV-Venus or AAV–APPsα–Venus DIV were transfected with the ER-targeted low-affinity GCaMP variant ER-GCaMP6-150 3 d before imaging using Lipofectamine.

SOCC experiments. The recording of Ca^{2+} signals following restoration of external Ca^{2+} are used to detect SOCC activity (25) that is crucial for ER store Ca^{2+} refilling (75). In acute rescue experiments, recAPPsα was used at a concentration of 10 nM or PBS for control.

Immunocytochemistry. Virally transduced cells, naïve hippocampal cultures, or cultures that underwent cTLP Ca^{2+} imaging with PBS or the recAPPsα peptide were fixed with 4% paraformaldehyde at DIV 14 to 16. Cells were permeabilized with 0.3% Triton X-100 in PBS (PBST) for 10 min, and unspecific binding was blocked with a 5% serum of primary antibody host in PBST 0.2% for 60 min. Neurons were incubated with primary antibodies diluted in blocking solution overnight followed by incubation with secondary antibodies (1:500, Jackson Laboratories): diluted in PBS for 2 h and counterstained with DAPI mounted with Fluoro-Gel (Electron Miscroscopy Sciences) onto glass slides for imaging.

Widefield Fluorescence Imaging and Analysis. Two-dimensional (2D) images were acquired using an upright Axio Imager M2 microscope (Zeiss) equipped with a 20× (protein expression) or oil-immersion objective (63× NA 1.4, receptor analysis) and a CCD camera.

Spontaneous calcium transients ex vivo. The imaging of spontaneous calcium transients of CA1 pyramidal neurons in acute hippocampal slices of LM control and NexCre cDKO animals from the same mice used for cLTP experiments was performed with the calcium indicator Fura2-AM.

Data Availability. All study data are included in the article and/or *SI Appendix*.

ACKNOWLEDGMENTS. We are grateful for the excellent technical assistance of Diane Mundil. In addition, we thank Christian J. Buchholz for providing viral vectors and Susanne Erdinger for excellent experimental help. Furthermore, we would like to thank Dr. Robert Blum for helpful suggestions regarding experimental design and data interpretation. We thank the German Research Foundation (DFG) for funding in the context of research group FOR1332 to U.C.M. and M.K. U.C.M. was supported by DFG Grant MU1457/14-1 and 15-1 and by the Else-Kröner Fresenius-Stiftung (2014-A229).

1. M. Agostini, C. Fasolato, When, where and how? Focus on neuronal calcium dysfunctions in Alzheimer's disease. *Cell Calcium* **60**, 289–298 (2016).
2. D. J. Surmeier *et al*., Calcium and Parkinson's disease. *Biochem. Biophys. Res. Commun.* **483**, 1013–1019 (2017).
3. H. Zhang *et al*., Calcium signaling, excitability, and synaptic plasticity defects in a mouse model of Alzheimer's disease. *J. Alzheimers Dis.* **45**, 561–580 (2015).
4. E. Popugaeva, E. Pchitskaya, I. Bezprozvanny, Dysregulation of neuronal calcium homeostasis in Alzheimer's disease–A therapeutic opportunity? *Biochem. Biophys. Res. Commun.* **483**, 998–1004 (2017).
5. M. J. Berridge, Calcium hypothesis of Alzheimer's disease. *Pflugers Arch.* **459**, 441–449 (2010).
6. A. Demuro, I. Parker, G. E. Stutzmann, Calcium signaling and amyloid toxicity in Alzheimer disease. *J. Biol. Chem.* **285**, 12463–12468 (2010).
7. U. C. Müller, T. Deller, M. Korte, Not just amyloid: Physiological functions of the amyloid precursor protein family. *Nat. Rev. Neurosci.* **18**, 281–298 (2017).
8. D. J. Selkoe, Alzheimer's disease is a synaptic failure. *Science* **298**, 789–791 (2002).
9. K. N. Green, F. M. LaFerla, Linking calcium to Abeta and Alzheimer's disease. *Neuron* **59**, 190–194 (2008).
10. I. Bezprozvanny, M. P. Mattson, Neuronal calcium mishandling and the pathogenesis of Alzheimer's disease. *Trends Neurosci.* **31**, 454–463 (2008).
11. K. Gazda, J. Kuznicki, T. Wegierski, Knockdown of amyloid precursor protein increases calcium levels in the endoplasmic reticulum. *Sci. Rep.* **7**, 14512 (2017).
12. S. Ring *et al*., The secreted beta-amyloid precursor protein ectodomain APPs alpha is sufficient to rescue the anatomical, behavioral, and electrophysiological abnormalities of APP-deficient mice. *J. Neurosci.* **27**, 7817–7826 (2007).
13. C. Zou *et al*., Amyloid precursor protein maintains constitutive and adaptive plasticity of dendritic spines in adult brain by regulating D-serine homeostasis. *EMBO J.* **35**, 2213–2222 (2016).
14. G. R. Dawson *et al*., Age-related cognitive deficits, impaired long-term potentiation and reduction in synaptic marker density in mice lacking the beta-amyloid precursor protein. *Neuroscience* **90**, 1–13 (1999).
15. S. W. Weyer *et al*., APP and APLP2 are essential at PNS and CNS synapses for transmission, spatial learning and LTP. *EMBO J.* **30**, 2266–2280 (2011).
16. B. Midthune *et al*., Deletion of the amyloid precursor-like protein 2 (APLP2) does not affect hippocampal neuron morphology or function. *Mol. Cell. Neurosci.* **49**, 448–455 (2012).
17. M. Hick *et al*., Acute function of secreted amyloid precursor protein fragment APPsα in synaptic plasticity. *Acta Neuropathol.* **129**, 21–37 (2015).
18. C. F. Stevens, J. F. Wesseling, Augmentation is a potentiation of the exocytotic process. *Neuron* **22**, 139–146 (1999).
19. S. Ludewig, M. Korte, Novel insights into the physiological function of the APP (gene) family and its proteolytic fragments in synaptic plasticity. *Front. Mol. Neurosci.* **9**, 161 (2017).
20. S. L. Cousins, S. E. Hoey, F. Anne Stephenson, M. S. Perkinton, Amyloid precursor protein 695 associates with assembled NR2A- and NR2B-containing NMDA receptors to result in the enhancement of their cell surface delivery. *J. Neurochem.* **111**, 1501–1513 (2009).
21. S. L. Cousins, W. Dai, F. A. Stephenson, APLP1 and APLP2, members of the APP family of proteins, behave similarly to APP in that they associate with NMDA receptors and enhance NMDA receptor surface expression. *J. Neurochem.* **133**, 879–885 (2015).
22. H.-S. Hoe *et al*., The effects of amyloid precursor protein on postsynaptic composition and activity. *J. Biol. Chem.* **284**, 8495–8506 (2009).
23. K. J. Lee *et al*., Beta amyloid-independent role of amyloid precursor protein in generation and maintenance of dendritic spines. *Neuroscience* **169**, 344–356 (2010).
24. R. Hamid *et al*., Amyloid precursor protein intracellular domain modulates cellular calcium homeostasis and ATP content. *J. Neurochem.* **102**, 1264–1275 (2007).
25. C. I. Linde, S. G. Baryshnikov, A. Mazzocco-Spezzia, V. A. Golovina, Dysregulation of Ca2+ signaling in astrocytes from mice lacking amyloid precursor protein. *Am. J. Physiol. Cell Physiol.* **300**, C1502–C1512 (2011).
26. E. Montagna *et al*., In vivo Ca^{2+} imaging of astrocytic microdomains reveals a critical role of the amyloid precursor protein for mitochondria. *Glia* **67**, 985–998 (2019).
27. M. A. Leissring *et al*., A physiologic signaling role for the gamma -secretase-derived intracellular fragment of APP. *Proc. Natl. Acad. Sci. U.S.A.* **99**, 4697–4702 (2002).
28. M. Chatzistavraki, E. Kyratzi, A. Fotinopoulou, P. Papazafiri, S. Efthimiopoulos, Downregulation of AβPP enhances both calcium content of endoplasmic reticulum and acidic stores and the dynamics of store operated calcium channel activity. *J. Alzheimers Dis.* **34**, 407–415 (2013).

29. R. Etcheberrigaray *et al*., Calcium responses in fibroblasts from asymptomatic members of Alzheimer's disease families. *Neurobiol. Dis.* **5**, 37–45 (1998).
30. H. Zhang, L. Wu, E. Pchitskaya, O. Zakharova, Neuronal store-operated calcium entry and mushroom spine loss in amyloid precursor protein knock-in mouse model of alzheimer's disease. *J. Neurosci.* **3535**, 13275–-13286 (2015).
31. K. V. Kuchibhotla *et al*., Abeta plaques lead to aberrant regulation of calcium homeostasis in vivo resulting in structural and functional disruption of neuronal networks. *Neuron* **59**, 214–225 (2008).
32. S. Sun *et al*., Reduced synaptic STIM2 expression and impaired store-operated calcium entry cause destabilization of mature spines in mutant presenilin mice. *Neuron* **82**, 79–93 (2014).
33. N. Arispe, E. Rojas, H. B. Pollard, Alzheimer disease amyloid beta protein forms calcium channels in bilayer membranes: Blockade by tromethamine and aluminum. *Proc. Natl. Acad. Sci. U.S.A.* **90**, 567–571 (1993).
34. F. M. LaFerla, Calcium dyshomeostasis and intracellular signalling in Alzheimer's disease. *Nat. Rev. Neurosci.* **3**, 862–872 (2002).
35. T. Tomita, Molecular mechanism of intramembrane proteolysis by γ-secretase. *J. Biochem.* **156**, 195–201 (2014).
36. X. Xu, Gamma-secretase catalyzes sequential cleavages of the AbetaPP transmembrane domain. *J. Alzheimers Dis.* **16**, 211–224 (2009).
37. D. Kögel, T. Deller, C. Behl, Roles of amyloid precursor protein family members in neuroprotection, stress signaling and aging. *Exp. Brain Res.* **217**, 471–479 (2012).
38. R. Fol *et al*., Viral gene transfer of APPsα rescues synaptic failure in an Alzheimer's disease mouse model. *Acta Neuropathol.* **131**, 247–266 (2016).
39. M. C. Richter *et al*., Distinct *in vivo* roles of secreted APP ectodomain variants APPsα and APPsβ in regulation of spine density, synaptic plasticity, and cognition. *EMBO J.* **37**, e98335 (2018).
40. V. T. Y. Tan *et al*, Lentivirus-mediated expression of human secreted amyloid precursor protein-alpha prevents development of memory and plasticity deficits in a mouse model of Alzheimer's disease. *Mol. Brain* **11**, 7 (2018).
41. S. Moosmang *et al*., Role of hippocampal Cav1.2 Ca2+ channels in NMDA receptor-independent synaptic plasticity and spatial memory. *J. Neurosci.* **25**, 9883–9892 (2005).
42. O. Thibault, R. Hadley, P. W. Landfield, Elevated postsynaptic [Ca2+]i and L-type calcium channel activity in aged hippocampal neurons: Relationship to impaired synaptic plasticity. *J. Neurosci.* **21**, 9744–9756 (2001).
43. G. E. Stutzmann *et al*., Enhanced ryanodine receptor recruitment contributes to Ca2+ disruptions in young, adult, and aged Alzheimer's disease mice. *J. Neurosci.* **26**, 5180–5189 (2006).
44. J. de Juan-Sanz *et al*., Axonal endoplasmic reticulum Ca^{2+} content controls release probability in CNS nerve terminals. *Neuron* **93**, 867–881.e6 (2017).
45. A. Ishida, K. Furukawa, J. N. Keller, M. P. Mattson, Secreted form of beta-amyloid precursor protein shifts the frequency dependency for induction of LTD, and enhances LTP in hippocampal slices. *Neuroreport* **8**, 2133–2137 (1997).
46. C. J. Taylor *et al*., Endogenous secreted amyloid precursor protein-alpha regulates hippocampal NMDA receptor function, long-term potentiation and spatial memory. *Neurobiol. Dis.* **31**, 250–260 (2008).
47. L. Moreno *et al*., sAβPPα improves hippocampal NMDA-dependent functional alterations linked to healthy aging. *J. Alzheimers Dis.* **48**, 927–935 (2015).
48. B. G. Mockett *et al*. Glutamate receptor trafficking and protein synthesis mediate the facilitation of ltp by secreted amyloid precursor protein-alpha. **39**, 3188–3203 (2019).
49. A. J. Borgdorff, D. Choquet, Regulation of AMPA receptor lateral movements. *Nature* **417**, 649–653 (2002).
50. C. Tardin, L. Cognet, C. Bats, B. Lounis, D. Choquet, Direct imaging of lateral movements of AMPA receptors inside synapses. *EMBO J.* **22**, 4656–4665 (2003).
51. S. Samtleben, B. Wachter, R. Blum, Store-operated calcium entry compensates fast ER calcium loss in resting hippocampal neurons. *Cell Calcium* **58**, 147–159 (2015).
52. M. Prakriya, R. S. Lewis, Store-operated calcium channels. *Physiol. Rev.* **95**, 1383–1436 (2015).
53. A. B. Parekh, J. W. Putney Jr, Store-operated calcium channels. *Physiol. Rev.* **85**, 757–810 (2005).
54. A. Skibinska-Kijek, M. B. Wisniewska, J. Gruszczynska-Biegala, A. Methner, J. Kuznicki, Immunolocalization of STIM1 in the mouse brain. *Acta Neurobiol. Exp. (Warsz.)* **69**, 413–428 (2009).
55. A. Berna-Erro *et al*., STIM2 regulates capacitive Ca2+ entry in neurons and plays a key role in hypoxic neuronal cell death. *Sci. Signal.* **2**, ra67 (2009).
56. M. Cameron *et al*., Calcium imaging of AM dyes following prolonged incubation in acute neuronal tissue. *PLoS One* **11**, e0155468 (2016).
57. G. E. Stutzmann, A. Caccamo, F. M. LaFerla, I. Parker, Dysregulated IP3 signaling in cortical neurons of knock-in mice expressing an Alzheimer's-linked mutation in presenilin1 results in exaggerated Ca2+ signals and altered membrane excitability. *J. Neurosci.* **24**, 508–513 (2004).
58. B. C.-K. Tong *et al*., Familial Alzheimer's disease-associated presenilin 1 mutants promote γ-secretase cleavage of STIM1 to impair store-operated Ca2+ entry. *Sci. Signal.* **9**, ra89 (2016).
59. W. Musleh, X. Bi, G. Tocco, S. Yaghoubi, M. Baudry, Glycine-induced long-term potentiation is associated with structural and functional modifications of alpha-amino-3-hydroxyl-5-methyl-4-isoxazolepropionic acid receptors. *Proc. Natl. Acad. Sci. U.S.A.* **94**, 9451–9456 (1997).
60. K. Michaelsen-Preusse *et al*., Neuronal profilins in health and disease: Relevance for spine plasticity and Fragile X syndrome. *Proc. Natl. Acad. Sci. U.S.A.* **113**, 3365–3370 (2016).
61. L. Bojarski *et al*., Presenilin-dependent expression of STIM proteins and dysregulation of capacitative Ca2+ entry in familial Alzheimer's disease. *Biochim. Biophys. Acta* **1793**, 1050–1057 (2009).
62. M. A. Leissring *et al*., Capacitative calcium entry deficits and elevated luminal calcium content in mutant presenilin-1 knockin mice. *J. Cell Biol.* **149**, 793–798 (2000).
63. B. Wang *et al*., The amyloid precursor protein controls adult hippocampal neurogenesis through GABAergic interneurons. *J. Neurosci.* **34**, 13314–13325 (2014).
64. E. Copanaki *et al*., The amyloid precursor protein potentiates CHOP induction and cell death in response to ER Ca2+ depletion. *Biochim. Biophys. Acta* **1773**, 157–165 (2007).
65. M. A. Busche *et al*., Critical role of soluble amyloid-β for early hippocampal hyperactivity in a mouse model of Alzheimer's disease. *Proc. Natl. Acad. Sci. U.S.A.* **109**, 8740–8745 (2012).
66. M. Calvo-Rodriguez, E. Hernando-Perez, L. Nuñez, C. Villalobos, Amyloid β oligomers increase ER-mitochondria Ca^{2+} cross talk in young hippocampal neurons and exacerbate aging-induced intracellular Ca^{2+} remodeling. *Front. Cell. Neurosci.* **13**, 22 (2019).
67. S. F. Santos *et al*., Expression of human amyloid precursor protein in rat cortical neurons inhibits calcium oscillations. *J. Neurosci.* **29**, 4708–4718 (2009).
68. G. Rojas *et al*., Effect of the knockdown of amyloid precursor protein on intracellular calcium increases in a neuronal cell line derived from the cerebral cortex of a trisomy 16 mouse. *Exp. Neurol.* **209**, 234–242 (2008).
69. N. J. Webster, M. Ramsden, J. P. Boyle, H. A. Pearson, C. Peers, Amyloid peptides mediate hypoxic increase of L-type Ca2+ channels in central neurones. *Neurobiol. Aging* **27**, 439–445 (2006).
70. T. S. Anekonda, J. F. Quinn, Calcium channel blocking as a therapeutic strategy for Alzheimer's disease: The case for isradipine. *Biochim. Biophys. Acta* **1812**, 1584–1590 (2011).
71. M. A. Lovell *et al*., Calcium channel blockers, progression to dementia, and effects on amyloid beta peptide production. *Oxid. Med. Cell. Longev.* **2015**, 787805 (2015).
72. L. Yang, Z. Wang, B. Wang, N. J. Justice, H. Zheng, Amyloid precursor protein regulates Cav1.2 L-type calcium channel levels and function to influence GABAergic short-term plasticity. *J. Neurosci.* **29**, 15660–15668 (2009).
73. D. Hefter, M. Kaiser, S. W. Weyer, I. E. Papageorgiou, M. Both, Amyloid precursor protein protects neuronal network function after hypoxia via control of voltage-gated calcium channels. *J. Neurosci.* **36**, 8356–8371 (2016).
74. B. G. Mockett, M. Richter, W. C. Abraham, U. C. Müller, Therapeutic potential of secreted amyloid precursor protein APPsα. *Front. Mol. Neurosci.* **10**, 30 (2017).
75. S. Ludewig "Functional importance of the APP/APLP protein family at the cellular and network level in the mouse central nervous system," PhD thesis,Technische Universtät Braunschweig (2017).
76. E. Danielson, S. H. Lee, SynPAnal: Software for rapid quantification of the density and intensity of protein puncta from fluorescence microscopy images of neurons. *PLoS One* **9**, e115298 (2014).